


Hyper-crosslinked 4-amino-1,8-naphthalimide Tröger's base containing pyridinium covalent organic polymer (COP) for discriminative fluorescent sensing of chemical explosives

Jason M. Delente , Deivasigamani Umadevi , Kevin Byrne , Wolfgang Schmitt , Graeme W. Watson , Thorfinnur Gunnlaugsson & Sankarasekaran Shanmugaraju


To cite this article: Jason M. Delente , Deivasigamani Umadevi , Kevin Byrne , Wolfgang Schmitt , Graeme W. Watson , Thorfinnur Gunnlaugsson & Sankarasekaran Shanmugaraju (2020): Hyper-crosslinked 4-amino-1,8-naphthalimide Tröger's base containing pyridinium covalent organic polymer (COP) for discriminative fluorescent sensing of chemical explosives, *Supramolecular Chemistry*, DOI: [10.1080/10610278.2020.1825715](https://doi.org/10.1080/10610278.2020.1825715)

To link to this article: <https://doi.org/10.1080/10610278.2020.1825715>

 [View supplementary material](#)

 Published online: 20 Oct 2020.

 [Submit your article to this journal](#)

 Article views: 18

 [View related articles](#)

 [View Crossmark data](#)



Hyper-crosslinked 4-amino-1,8-naphthalimide Tröger's base containing pyridinium covalent organic polymer (COP) for discriminative fluorescent sensing of chemical explosives

Jason M. Delente^{a,b}, Deivasigamani Umadevi^c, Kevin Byrne^c, Wolfgang Schmitt^{b,c}, Graeme W. Watson^c, Thorfinnur Gunnlaugsson^{a,b} and Sankarasekaran Shanmugaraju^d

^aSchool of Chemistry and Trinity Biomedical Sciences Institute, Trinity College Dublin, The University of Dublin, Dublin, Ireland; ^bSchool of Chemistry and Centre for Research on Adaptive Nanostructures and Nanodevices (CRANN), Trinity College Dublin, the University of Dublin, Dublin, Ireland; ^cDiscipline of Chemistry, Indian Institute of Technology, Palakkad, India; ^dAMBER (Advanced Materials and Bioengineering Research) Centre, Trinity College Dublin, The University of Dublin, Dublin, Ireland

ABSTRACT

A new hyper-crosslinked 4-amino-1,8-naphthalimide Tröger's base containing pyridinium covalent organic polymer, **TBNap-COP**, was synthesised and employed as a 'turn-off' fluorescent chemosensor for nitroaromatic explosives. **TBNap-COP** was synthesised in quantitative yield using a one-step nucleophilic substitution reaction between a dipyrindyl scaffold (**TBNap**, bis-[N-(2-(pyridine-4-yl)ethyl)]-9,18-methano-1,8-naphthalimide-[b,f][1,5]diazocine) and 1,3,5-tris(bromomethyl)benzene by heating in DMF for 3 days. The formation and phase-purity of **TBNap-COP** were fully characterised by using various spectroscopic and microscopy analyses. The suspension of **TBNap-COP** in water showed strong fluorescence emission characteristics owing to the 'push-pull' based ICT transition and it was used as a fluorescent sensor for discriminative detection of nitroaromatic explosives. **TBNap-COP** displayed selective fluorescence quenching responses for phenolic-nitroaromatics, with particularly high sensitivity for picric acid which is a powerful secondary chemical explosive and a harmful environmental pollutant widely used in the dye industries.

ARTICLE HISTORY

Received 11 August 2020
Accepted 11 September 2020

KEYWORDS


Organic polymers; Tröger's base; 1,8-naphthalimide; fluorescence; chemosensing; nitroaromatics

Introduction

The development of suitable sensors and probes for fast and reliable identification of chemical explosives at trace-level is necessary to combat terrorism, improve homeland security, and to eliminate environmental pollution [1,2]. Nitroaromatic compounds (NACs), such as 2,4,6-trinitrotoluene (TNT) and the related 2,4,6-trinitrophenol also known as picric acid (PA), are classified as powerful secondary chemical explosives because of their high detonation velocity [3]. Due to their low-cost preparation and easy transportation, NACs are used as the primary component in various known chemical explosives [4,5]. For example, Tritonal is a well-known chemical explosive made up of 80% TNT and 20% aluminium powder [3–5]. However, apart from their use as a powerful chemical explosive, many of these electron-deficient structures have other 'chemical' roles and functions, for instance in chemical biology, where agents such as 2,4-dinitrophenol (DNP) can inhibit adenosine triphosphate (ATP) production in cells [6]. Hence, many

NACs can have high acute toxicity. Other NACs, such as the aforementioned PA, are also extensively used as a reagent in the pharmaceutical industry and as a yellow pigment in the dye industry [2–5]. This makes PA highly available and accessible, which is concerning. PA is a very common reagent, being environmental contaminant and toxic to living organisms [3–5,7]. Because of its extensive use, and high solubility in water ($\sim 14 \text{ g.L}^{-1}$), PA and its derivatives can easily contaminate groundwater and soils, exposing humans and animals/life-stocks [5,7]. In fact, continuous exposure to saturated vapours of PA can cause severe eye irritation and headaches, while prolonged exposure results in serious and irreversible health issues like liver and kidney failure, and neurological damage [3–5,7]. Hence, there is a need to develop a suitable and reliable sensor for the trace detection of NACs. Various techniques for detection are currently used but are often very expensive and have limited portability, making them impractical for on-site detection [8]. Therefore, researchers have directed their efforts towards fluorescence sensors representing

CONTACT Thorfinnur Gunnlaugsson ✉ gunnlaut@tcd.ie School of Chemistry, Trinity Biomedical Sciences Institute and AMBER (Advanced Material and Bioengineering Research) Centre, Trinity College Dublin, The University of Dublin, Dublin 2, Ireland; Shanmugaraju Sankarasekaran shanmugam@iitpkd.ac.in Department of Chemistry, Indian Institute of Technology, Palakkad, Kerala, India

 Supplemental data for this article can be accessed [here](#).

a low-cost sensing method with high sensitivity and selectivity and are often synonym of portable devices for on-site detections [1–7], and this is an area we have been developing in recent times [9,10].

A wide variety of fluorophores have been used, ranging from purely organic molecules to inorganic and hybrid compounds such as tetraphenylethenes [11], pentacenequinones [12], carbazoles [13], pyrene [14], calixarene [15], Tröger's base [16], 1,8-naphthalimides [17], quantum dots [18], metal-organic frameworks (MOFs) [19], and covalent organic polymers [20]. Amongst the plethora of sensors created, polymer-based sensors are advantageous because of their enhanced sensitivity caused by the signal amplification effect and recyclability [21]. Covalent organic polymers (COPs) are a class of porous polymers gaining significant interest as chemosensors for the trace detection of environmental pollutants and hazardous substances [22]. Like MOFs, COPs are also composed of repeating motifs but only contain organic functional groups, usually leading to materials that are lighter than MOFs, as they are mainly composed of light elements (C, H, N, O) [23]. COPs are also generally very robust as they are principally composed of C–C and C–N bonds [24]. In a similar fashion to MOFs, it is possible to control the pore size and therefore, the surface area of the polymer [25]. Most COPs synthesised are used for gas storage and catalysis; however, the luminescent properties of these materials, combined with the ability to tune their pore sizes, make them ideal candidates for sensing applications [26].

Using electron-rich, conjugated fluorophores as one of the COP building blocks leads to the formation of large π -conjugated networks, which are capable of acting as excellent electron donors that exhibit increased sensitivity towards electron acceptor analytes such as nitroaromatics [9,21,25,26]. Taking into account these considerations, and knowledge gained from previous results from our laboratory showing that 4-amino-1,8-naphthalimide-Tröger's base (**TBNaps**) can discriminatively detect chemical explosives with high sensitivity [9,10], we report herein a novel hyper-crosslinked 4-amino-1,8-naphthalimide-Tröger's base functionalised pyridinium covalent organic polymer **TBNap-COP**. Our approach is based on three factors: (i) By using a **TBNap** moiety we take advantage of the presence of the Lewis basic nitrogen's of the Tröger's base motif, which should lead to good selectivity and sensitivity towards phenolic nitroaromatics particularly for PA; (ii) By using 1,3,5-trimethyl benzene as the linking point between each **TBNap** this should lead to a hyper-crosslinked polymeric system, which could potentially further increase the sensitivity by providing additional binding sites; (iii) The presence of positively charged pyridinium ions and

the bromide anions should help to solvate the polymer, countering any π - π stacking interactions taking place, and thus facilitating the formation of a very stable fine suspension of **TBNap-COP** in water. As we expected **TBNap-COP** exhibited enhanced fluorescence emission when dispersed in water. However, as we demonstrate here, the screening of the solution of structurally close-related NACs resulted in significant quenching in the **TBNap-COP** emission, the largest quenching response being observed for PA, which also displayed a discriminative sensing propensity towards phenolic NACs over non-phenolic NACs.

Experimental section

Materials and methods

All reagents, solvents, starting materials, and nitroaromatic analytes were purchased from Sigma-Aldrich, Merck, or Fisher Scientific and were of reagent grade and were used as received. Solvents used were HPLC grade unless otherwise stated. Deuterated solvent ($(\text{CD}_3)_2\text{SO}$) used for NMR analyses was purchased from Sigma-Aldrich or Apollo Scientific. The monomer **TBNap** was synthesised according to the previously published procedure [27,28]. (Caution! Nitroaromatic analytes are classified as secondary chemical explosives and should be handled only in small quantity).

The elemental analysis for C, H, and N was performed on an Exeter analytical CE-450 elemental analyser.

FT-IR spectra were recorded in the range 4000–550 cm^{-1} on a Perkin-Elmer spectrometer equipped with a universal ATR sampling accessory.

The solution-phase ^1H NMR spectra were recorded at 400 MHz using an Agilent Technologies 400-MR NMR spectrometer. Chemical shifts are reported in ppm with the deuterated solvents as the internal reference. All NMR spectra were carried out at 293 K. The ^{13}C NMR spectra of precursors were acquired in $\text{DMSO}-d_6$ at 100.55 MHz at 25°C.

The solid-state CP/MAS ^{13}C NMR spectrum of **TBNap-COP** was acquired at 201.1 MHz using a 3.2 mm double-resonance MAS probe. The spectrum was acquired under magic angle spinning (MAS) at 20 kHz, if not otherwise specified, using ramped-amplitude cross-polarisation, and SPINAL64 decoupling with a ^1H -decoupling field of about 80 kHz. A 3 ms contact time and a pulse delay of 5 s were used. Chemical shifts were calibrated setting the ^{13}C low field signal of adamantane to 8.48 ppm.

Mass spectrometry was carried out using HPLC grade solvents. Electrospray mass spectra were determined on a Micromass LCT spectrometer and high-resolution mass

spectra were determined relative to a standard of leucine enkephaline. MALDI-Q-TOF mass spectra were carried out on a MALDI-Q-TOF-premier and high-resolution mass spectrometry was performed using Glu-Fib with an internal reference peak of m/z 1570.6774.

Morphology of **TBNap-COP** was imaged using field emission scanning electron microscopy (FE-SEM) with an SE2 on the in-lens detector. The sample was prepared by drop-casting the aqueous suspension (1 mg in 100 μL of Millipore water) of as-synthesised **TBNap-COP** on silica wafers, then coated with Au and dried under vacuum before the imaging.

UV-visible absorption spectra were recorded in 1 cm quartz cuvettes (Hellma) on a Varian Cary 50 spectrometer. Baseline correction was applied for all spectra.

Emission spectra were recorded on a Varian Cary Eclipse Fluorimeter. The temperature was kept constant throughout the measurements at 298 K by using a thermostatic unit block.

Synthesis of pyridinium polymer **TBNap-COP**

A mixture of monomers *bis*-[N-(2-(pyridine-4-yl)ethyl)]-9,18-methano-1,8-naphthalimide-*[b,f]* [1,5]diazocine (**TBNap**, 150 mg, 0.22 mmol, 3.0 eq.) and 1,3,5-Tris(bromomethyl)benzene (53 mg, 0.15 mmol, 2.0 eq.) was taken in a Pyrex tube along with 50 mL of DMF. Then, the mixture was heated under stirring at 100°C for 3 days. The formed heavy precipitate was isolated by vacuum filtration and then the precipitate was washed extensively with DCM (2 \times 50 mL), CH₃OH (2 \times 50 mL) and diethyl ether (1 \times 50 mL) to remove the unreacted monomers and oligomers. Finally, the solid was dried under high vacuum for 6 hours to isolate the expected pyridinium covalent organic polymer **TBNap-COP** as bright yellow powder (68%). Elemental analysis (%) calculated for the repeating unit 3CH₂Cl₂.4CH₃OH.DMF: C, 56.99; H, 4.33; N, 8.36; found: C, 56.79, H, 4.18, N, 8.45; FT-IR (ν cm⁻¹): 3371, 2972, 1691, 1654, 1595, 1570, 1511, 1458, 1402, 1376, 1342, 1300, 1259, 1231, 1169, 1151, 1126, 1090, 1053, 921, 870, 785, 759, 693; ¹H NMR (400 MHz, (CD₃)₂SO) δ 11.61 (4 H, s, pyridyl-H), 8.75–8.72 (2 H, d, J = 8.0 Hz, Ar-H), 8.48–8.46 (2 H, d, J = 8.0 Hz, Ar-H), 8.10 (2 H, s, Ar-H), 8.06 (3 H, s, Ph-H), 7.99–7.95 (2 H, t, J = 8.0 Hz, Ar-H), 7.40 (4 H, s, pyridyl-H), 5.19–5.15 (2 H, d, J = 16.0 Hz, N-CH₂), 4.71 (8 H, m, N-CH₂, Ph-CH₂), 4.66 (2 H, s, N-CH₂), 4.29–4.26 (4 H, t, J = 12.0 Hz, CH₂-CH₂), 3.00–2.97 (4 H, t, J = 12.0 Hz, CH₂-CH₂).

Gas uptake measurements

All the gas (N₂, H₂, and CO₂) adsorption measurements were carried out using a Quantachrome Autosorb IQ automated gas sorption analyser. The as-synthesised

TBNap-COP was immersed in diethyl ether for 3 days. During the immersion, the diethyl ether was refreshed 5 times with fresh diethyl ether and the resulting solvent exchanged polymer was transferred to a quartz cell. The sample was evacuated under vacuum at 100°C for 72 hours. BOC gases ultrahigh-purity grade N₂, H₂, and CO₂ were used in all adsorption measurements. The surface area of **TBNap-COP** was calculated by the Brunauer-Emmett-Teller (BET) method.

Preparation of the stock solution

10 mg of **TBNap-COP** was placed in a 10 mL standard measuring flask and 100 mL of respective solvents were added to it. Then, the mixture was sonicated for 30 minutes and aged for 72 h to get a uniform suspension for spectroscopic studies. The desired quantity of each of the nitroaromatics was dissolved into 2 mL of EtOH and then 18 mL of deionised water was slowly added to the solution.

Fluorescence titration experiments

200 μL of the suspension of **TBNap-COP** in water was taken in a quartz cuvette and 1800 μL of water was added to it. During the fluorescence titration, 1 mM solution of different nitroaromatic explosives was added (0.0 μM – 90.9 μM) in an incremental fashion (20 μL each addition) to a 2 mL aqueous suspension of **TBNap-COP**. The emission intensity was monitored after each addition. For all the fluorescence titration experiments, the excitation wavelength was 380 nm and the emission spectra were recorded in the range of 400–800 nm. The percentage of quenching efficiency was calculated from the following equation:

$$\text{Quenching efficiency}(\%) = (I_0 - I)/I_0 \times 100$$

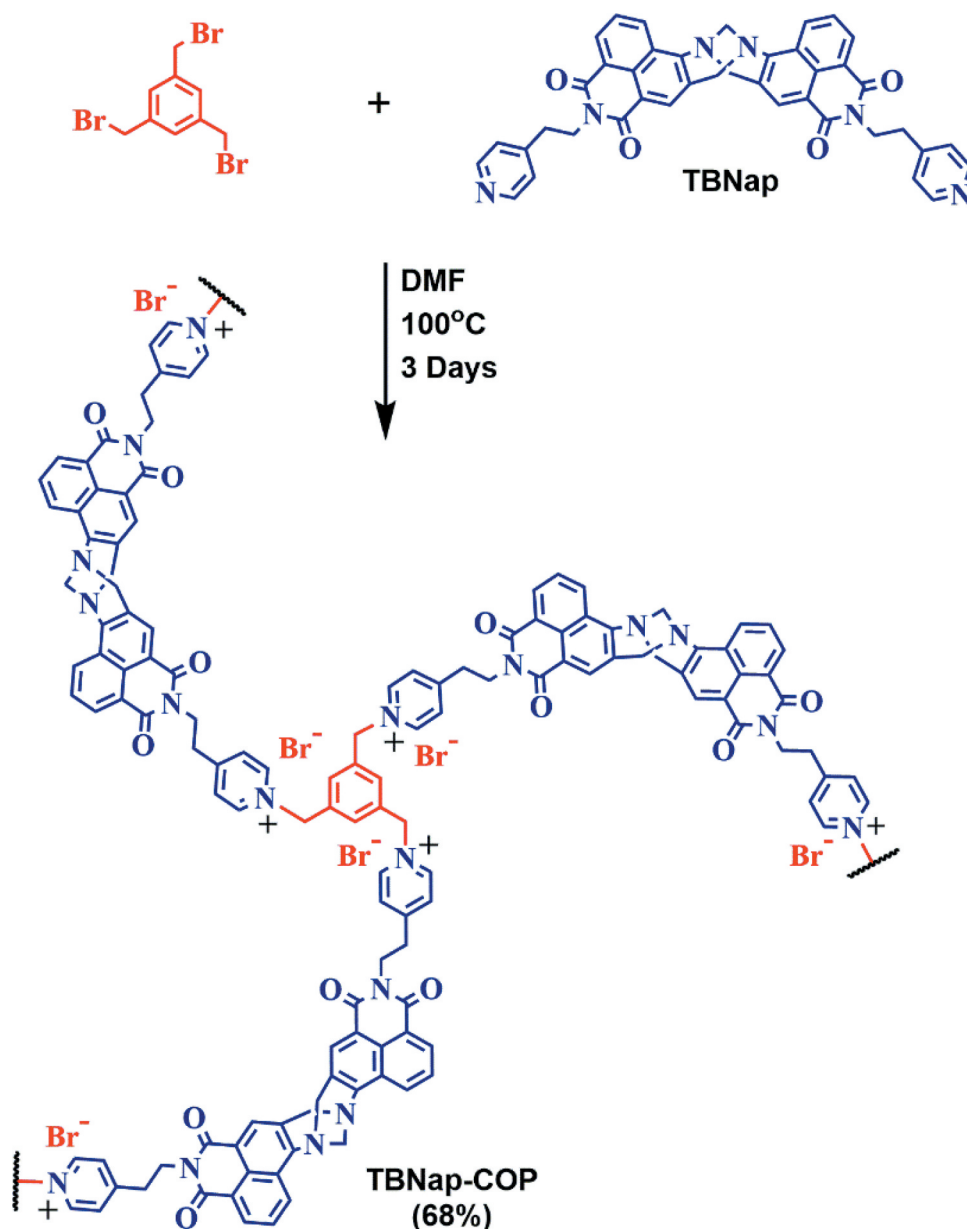
Where I_0 is the initial emission intensity of **TBNap-COP** in H₂O and I is the intensity after the addition of the analyte.

Results and discussion

Synthesis and characterisation of **TBNap-COP**

As shown in Scheme 1, the polymer **TBNap-COP** was readily synthesised in quantitative yield (68%) using **TBNap** and the commercially available 1,3,5-tris(bromomethyl)benzene by heating in DMF for 3 days.

The successful formation of **TBNap-COP** was confirmed by ¹H NMR, solid-state CP-MAS ¹³C NMR, FT-IR, and elemental analysis. The ¹H NMR spectrum in DMSO-d₆ revealed the presence of the Tröger's base



Scheme 1. Synthesis of pyridinium covalent organic polymer TBNap-COP.

moiety with the doublet at 5.19 ppm and the merged singlet and doublet at 4.71–4.66 ppm accounting for the methylene protons of the diazocine ring (Figure S1) [9,10,27]. Notably, the pyridyl ^1H signals of **TBNap-COP** are significantly down-field shifted (~ 3.14 ppm) upon quaternization. The solid-state CP-MAS ^{13}C -NMR spectrum further confirmed the presence of the **TBNap** unit, with a resonance at 164 ppm corresponding to the carbonyl groups, and two further resonances at 64 ppm and 57 ppm ascribed to the CH_2 of the diazocine ring (Figure S1) [9,10]. The FT-IR spectrum of **TBNap-COP** showed two signals at 1691 cm^{-1} and 654 cm^{-1} corresponding to the carbonyl ($\text{C}=\text{O}$) groups of the naphthalimide moiety, two strong transitions at

1259 cm^{-1} and 1231 cm^{-1} accounting for the C-N stretching of the diazocine ring of the Tröger's base (Figure S2) [9,10,24]. Thermogravimetric analysis (TGA) of **TBNap-COP** under N_2 showed a weight loss of 4% at 200°C , representing the loss of solvent trapped within the polymeric network. **TBNap-COP** was found to be stable up to $\sim 270^\circ\text{C}$, demonstrating good thermal stability (Figure S3). The powder X-ray diffraction (PXRD) measurement confirmed that **TBNap-COP** is an amorphous solid (Figure S4), which was further supported by the scanning electron microscopy, where the solid forms aggregate with a random distribution of pores of various sizes (Figure 1). The gas uptake capacity of the as-synthesised polymer was investigated and the

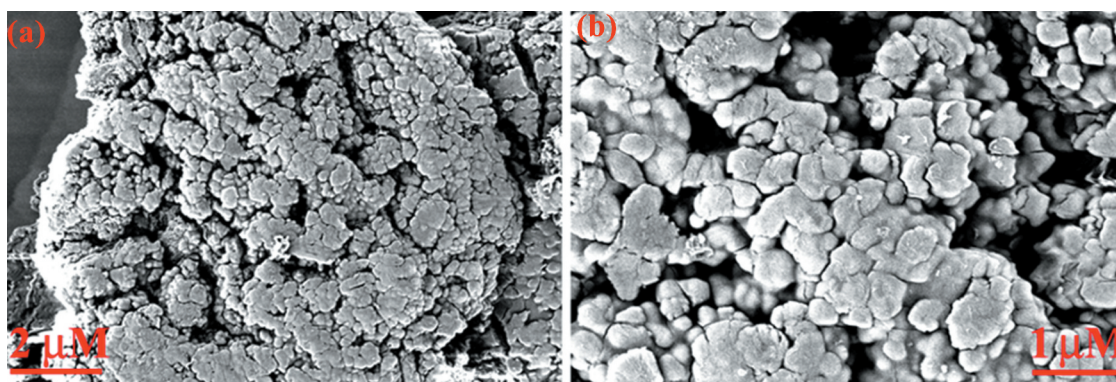


Figure 1. (a) Scanning electron microscopy image and (b) an enlarged image of the as-synthesised polymer **TBNap-COP**.

N_2 adsorption isotherm demonstrated reversible adsorption at 77 K of $55 \text{ cm}^3/\text{g}$ at 1 bar and the Brunauer-Emmett-Teller (BET) surface area was calculated to be $65 \text{ m}^2/\text{g}$ (Figure S5-S6). In addition to this study, the CO_2 adsorption was also studied but was found to be negligible.

Fluorescence sensing studies of **TBNap-COP**

Having successfully synthesised and characterised it, we then assessed the spectroscopic properties of **TBNap-COP**, particularly concerning its use as a fluorescence sensor for NACs by carrying out spectroscopic titrations in competitive aqueous media. The **TBNap-COP** showed the appearance of typical internal charge transfer (ICT, due to the push-pull nature of the naphthalimide moieties in the **TBNap** structure) transition with an absorption maxima in the visible region around $\lambda_{\text{max}} = 366 \text{ nm}$, and a broad emission band with λ_{max} at ca. 490 nm in water (Figure S7). To demonstrate the ability of **TBNap-COP** for sensing NACs, we performed a fluorescence titration study of **TBNap-COP** with PA as a prototype

of NACs. As shown in Figure 2, the initial emission intensity of **TBNap-COP** decreased progressively upon the incremental addition ($20 \rightarrow 200 \text{ } \mu\text{L}$) of PA (1 mM) solution in water. Except for a strong fluorescence quenching, no other significant spectral changes (such as a shift in λ_{max}) were observed. As it is shown in the inset of Figure 2, it is also possible to visually observe the quenching of the **TBNap-COP** fluorescence upon UV ($\lambda = 360 \text{ nm}$) irradiation, making **TBNap-COP** a good candidate for visual detection of PA. The observed change in emission intensity was further analysed by fitting the titration data to the classical Stern-Volmer equation ($I_0/I = 1 + K_{\text{SV}}[Q]$), from which the Stern-Volmer constant (K_{SV}) was determined. The quenching of the fluorescence upon the addition of PA follows a linear trend for the lower concentration while at higher concentration the curve rises exponentially signifying that a super-amplified quenching effect operates at higher concentration of PA (Inset in Figure 2). Therefore, the Stern-Volmer binding constant, $K_{\text{SV}} = 32.7 \pm 1.34 \times 10^3 \text{ M}^{-1}$, was determined at lower concentrations of PA, demonstrating the higher binding propensity of **TBNap-COP** and the obtained K_{SV}

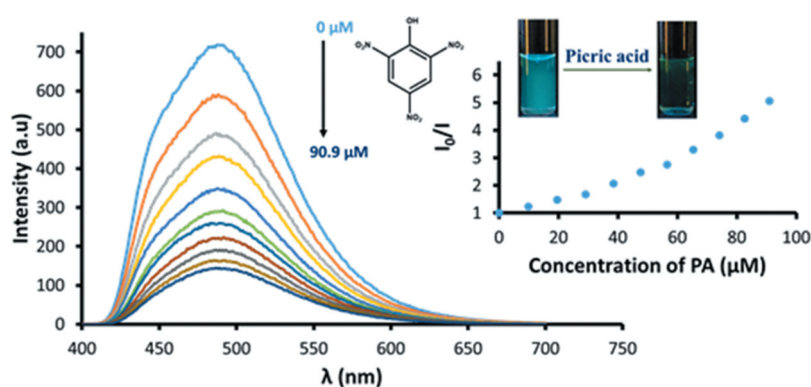


Figure 2. Fluorescence quenching of **TBNap-COP** upon the addition of PA (inset: its corresponding non-linear Stern-Volmer plot and visual colour change before and after the addition of PA under UV lamp).

is comparable to that which has been observed for similar systems (see Table S1).

Mechanism of fluorescence quenching

The obtained non-linear Stern-Volmer plot suggests that the fluorescence quenching could be the results of several mechanisms taking place: (i) energy transfer from the excited donor to an acceptor through a non-radiative pathway, (ii) the inner filter effect (IFE) due to the spectral overlap between the absorbance spectra of PA and the excitation spectra of **TBNap-COP**, (iii) the formation of hydrogen bonding interaction between the Lewis basic nitrogen of the Tröger's base and the hydroxy group of PA leading to the formation of a charge-transfer complex resulting in drastic quenching of emission intensity [9,10,24]. As seen in the superposition of the normalised absorbance spectrum of PA and the excitation and emission spectra of **TBNap-COP** (Figure S8), the inner filter effect is taking place and absorb part of the excitation light. However, this superposition also highlights a spectral overlap between the absorbance spectrum of PA and the emission spectrum of **TBNap-COP** confirming the possibility of energy transfer from the excited **TBNap-COP** to PA [1,2,9]. To estimate the participation of the IFE through the entire titration, the IFE correction was calculated using the equation:

$$I_{\text{corr}} = I_{\text{obs}} \times 10^{(A_{\text{ex}}+A_{\text{em}})/2}$$

Where I_{corr} is the corrected fluorescence intensity, I_{obs} the measured maximum intensity, A_{ex} and A_{em}

correspond to the absorbance values of **TBNap-COP** in presence of PA at the excitation wavelength and the maxima of emission, respectively [29,30].

The value for I_{corr} can be found in Table S2 and was used to determine the contribution of the IFE to the quenching efficiency. The contribution of the IFE was determined to be responsible for ~56% of the observed quenching efficiency in presence of 90.9 μM of PA (Figure S9). Thus, demonstrating that the inner filter effect is not the only mechanism responsible for the quenching of the emission intensity of **TBNap-COP** and that the remaining 24% of fluorescence quenching involves other mechanisms. The obtained non-linear Stern-Volmer plot suggests that the observed fluorescence quenching is presumably due to the combination of IFE and either static or dynamic quenching. This can be confirmed by analysing the time-resolved fluorescence decay profile of **TBNap-COP** before and after the addition of PA. These fluorescence decay measurements data of **TBNap-COP** in water were best fitted to a bi-exponential decay, from which excited state lifetimes (τ_1 and τ_2) of 3.97 ns and 10.61 ns, were determined, respectively. Upon the incremental addition of PA, the initial life-time of **TBNap-COP** decreased to 3.16 ns and 9.98 ns for τ_1 and τ_2 , respectively, (Figure 3). This demonstrates that PA is forming a complex with the excited state of **TBNap-COP** and that therefore dynamic quenching is taking place at higher concentrations of PA [9,10]. We also carried out temperature-dependent emission studies. These experiments demonstrated an increase in the quenching efficiency upon increasing the temperature, due to the enhanced

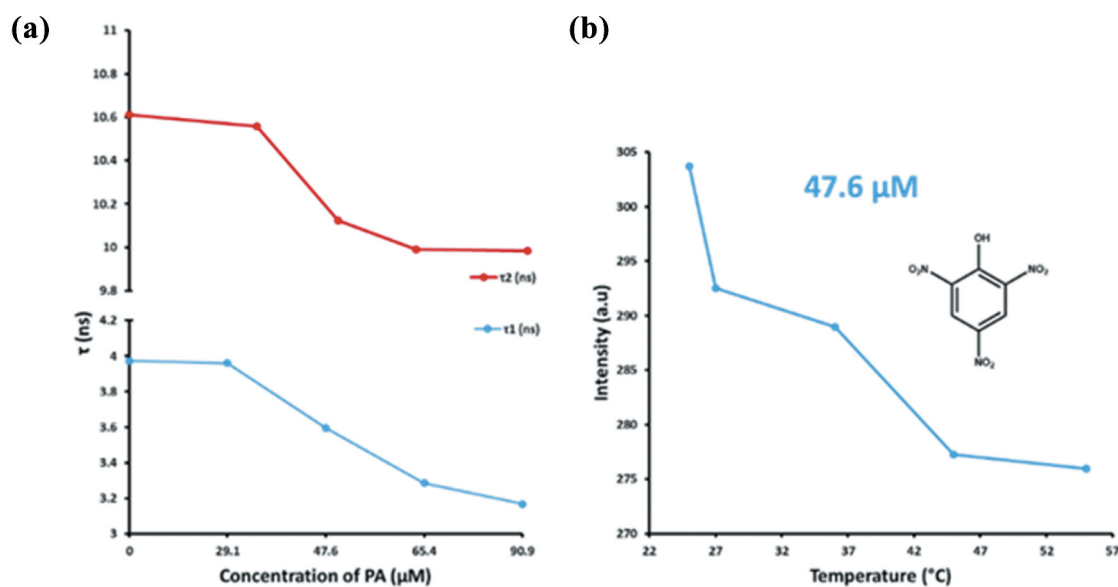


Figure 3. (a) Fluorescence decay profiles of **TBNap-COP** upon addition of PA (0 – 90.9 μM) and (b) its temperature-dependent emission profile in the presence of PA (47.6 μM).

molecular collision, of PA (47.6 μM) from 57% at 25°C to 61% at 55°C further confirming that the observed fluorescence quenching follows the dynamic quenching mechanism at higher NACs concentration (Figure 3) [9,10]. Furthermore, in the UV-vis absorption titrations studies, a significant increase in the absorption intensity of **TBNap-COP** upon the gradual mixing of PA was observed. However, no significant changes in the absorption maxima (λ_{max}) or no new peak were seen in the absorption spectra, which eliminate the possibility of ground-state charge transfer (CT) complexation between **TBNap-COP** and PA; this results further supported that PA forms a complex with the excited state **TBNap-COP** (Figure S10).

Theoretical study

To further understand the mechanism of excited-state charge transfer between **TBNap-COP** and picrate anion, theoretical calculations were undertaken by employing density functional theory (DFT). One monomer unit was considered as a model to represent the polymer. Geometry optimisations were performed using the M06-2X12 hybrid functional of Truhlar and Zhao with the 6-31 + G(d) basis set [31]. All the calculations were utilised in the Gaussian 09 package [32]. Figure 4 depicts the optimised geometry and the frontier orbitals of PA,

the picrate anion, and the **TBNap-COP** model system. The highest occupied molecular orbital (HOMO) of **TBNap-COP** was mainly located on the Tröger's base moiety and the lowest unoccupied molecular orbital (LUMO) density was more localised in the pyridinium moiety. The energy of the HOMO and the LUMO of the **TBNap-COP** model systems are -10.548 eV and -5.704 eV, respectively. The HOMO and LUMO of the picrate anion are -4.490 eV and 1.351 eV, respectively. This would suggest that charge transfer can occur from the HOMO of the picrate anion to the LUMO of **TBNap-COP** and supports the proposed excited-state charge-transfer quenching mechanism [33,34].

Selectivity and competitive studies

To explore the selectivity of **TBNap-COP** towards NACs, similar fluorescence titration studies, under identical experimental conditions, were performed with various interfering nitroaromatics. These studies revealed a differential fluorescence quenching responses of **TBNap-COP** for different NACs and thus, structurally similar nitro explosives can be discriminated based on their quenching propensity. As it is shown in Figure 5(a), upon the incremental addition (20 \rightarrow 200 μL) of different NACs (1 mM) in an aqueous suspension of **TBNap-COP**, a strong fluorescence quenching was observed for PA,

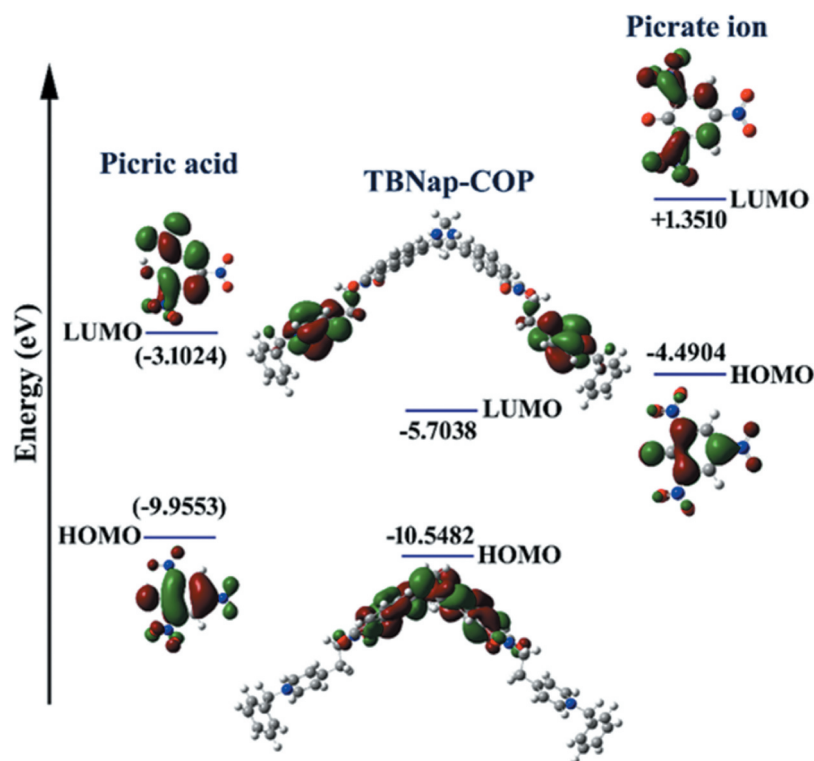


Figure 4. Pictorial representation of the charge transfer phenomena occurring from the HOMO of picrate ion to the LUMO of **TBNap-COP**.

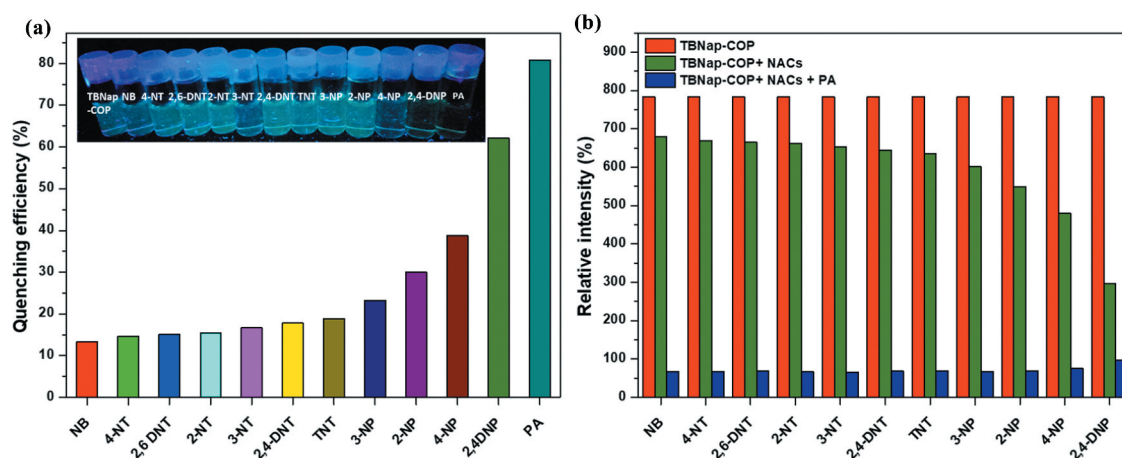


Figure 5. (a) Fluorescent quenching of **TBNap-COP** observed upon addition of different NACs (Insert: observed visual colour change before and after the addition of PA under UV lamp). (b) Competitive selective binding of **TBNap-COP** towards different NACs in the presence of PA in water.

2,4-dinitrophenol (2,4-DNP) and 4-nitrophenol (4-NP) with a quenching efficiency of 80%, 62%, and 39%, respectively. The highest quenching efficiency for PA is due to its more electron-deficient nature. The fluorescence titration experiments, which were shown to be fully reproducible, also highlighted the capacity of **TBNap-COP** to discriminate phenolic nitroaromatics over non-phenolic nitroaromatics. The observed discriminative fluorescence sensing is also being seen by visual colour changes as is given in Figure 5(a). The changes in the **TBNap-COP** emission upon the addition of different NACs are presented in Figure S11-S21. The Stern-Volmer constant for the other NACs titrations were also determined using the same method and are summarised in Table S3. From the analysis of the titration data, the order of decreasing quenching efficiency was determined as being: PA > 2,4-DNP > 4-NP > 2-NP > 3-NP > TNT > 2,4-DNT > 3-NT > 2-NT > 2,6-DNT > 4-NT > NB; being in a similar order to that seen previously for such systems [9,10]. These results demonstrate the high selectivity and discriminative sensing ability of **TBNap-COP** for phenolic-nitroaromatics over other interfering non-phenolic analytes. This favoured binding affinity is ascribed to the Lewis basic nitrogens of the Tröger's base moiety, interacting strongly with the acidic hydroxy groups of the phenolic-nitroaromatics in the sensing process [9,10,24].

To further validate the potential of **TBNap-COP** to act as a selective sensor, a competitive sensing experiment/titrations were performed in competitive media, where to an aqueous suspension of **TBNap-COP** (red bar), 90.9 μM of each of the NAC tested above was added (green bar) and the emission spectra were recorded

(Figure 5(b)). This was then followed by the addition of 90.9 μM of PA (blue bar), and the emission spectra were recorded. A strong quenching of emission intensity of **TBNap-COP** (in presence of NACs) was observed after the addition of PA. To demonstrate the high selectivity of **TBNap-COP** for PA further, a similar competitive study was performed in the presence of group-I and transitions metal ions commonly present in water. **TBNap-COP** showed the highest binding propensity for PA in the presence of these different metal cations (Figure S22) demonstrating the ability of **TBNap-COP** to selectively detect the presence of PA in aqueous media in co-existence of other structurally similar and potentially competing analytes. The influence of pH on the sensing propensity was also investigated and it showed sensitivity to pH (Figure S23). Indeed, in acidic conditions (pH = 2.3), the binding capacity was slightly decreased ($K_{SV} = 2.35 \pm 0.05 \times 10^4 \text{ M}^{-1}$), but in basic medium (pH = 11.7) the capacity is drastically decreased ($K_{SV} = 1.86 \pm 0.06 \times 10^4 \text{ M}^{-1}$) presumably due to the diminished intermolecular interactions, as proposed earlier, between **TBNap-COP** and NACs at alkaline pH [9,10,24].

Sensitivity and response time

One important parameter for on-site detection/sensing is a fast time of response, which corresponds to how long the system needs to be exposed to an analyte before the detection takes place. The time of response of **TBNap-COP** was tested in the presence of PA at different concentrations, and this experiment demonstrated that the maximum quenching response is reached within one minute of contact time with PA.

Thus, **TBNap-COP** can be an excellent sensor for the fast detection of NACs (Figure S24). To find out the sensitivity of **TBNap-COP** for NAC detection, the limit of detection was estimated at natural pH. The sensitivity experiment showed that the fluorescence of **TBNap-COP** was affected by a quantity as low as 12 ppb of PA, making this system a very sensitive and selective sensor for PA (Figure S25). Moreover, this level of sensitivity is below the allowed limit of NACs in drinking water established by the US EPA [6,7,11,12].

Conclusion

In summary, we have synthesised a new **TBNap** functionalised pyridinium covalent organic polymer and demonstrated its uses as a fluorescent sensor for NACs. More importantly, it was demonstrated that **TBNap-COP** exhibited a rapid fluorescence quenching response for PA exposure and was able to selectively sense PA, even in the presence of other competing analytes. This system has proven to be very sensitive towards traces of PA, making it an ideal candidate for on-site detection of PA. We are currently developing the application of **TBNap-COP** further to design a practically feasible sensor system.

Acknowledgments

We thank the Irish Research Council (IRC) (GOIPD/2015/290 to D. U.), Science Foundation Ireland (SFI PI Award 13/IA/1865 to TG and 13/IA/1896 to WS) and European Research Council (CoG SUPRAMOL 2014–647719 to WS) and Science and Engineering Research Board (EMEQ Award EEQ/2018/000799 to SS) for financial support. Computational calculations were performed using the Lonsdale supercomputing at Trinity Centre for High-performance Computing (TCHPC). We thank Drs J. E. O'Brien, M. Reuther, and G. Hessman for NMR and MS analysis. SEM analysis was performed at the AMBER Center and the CRANN Advanced Microscopy Laboratory (AML), TCD.

Disclosure statement

There are no conflicts to declare.

Funding

This work was supported by the H2020 European Research Council [CoG SUPRAMOL 2014–647719 to W.S.]; Science and Engineering Research Board [EMEQ Award EEQ/2018/000799 to SS].

ORCID

Jason M. Delente  <http://orcid.org/0000-0002-8889-5798>

References

- [1] Sun X, Wang Y, Lei Y. Fluorescence based explosive detection: from mechanisms to sensory materials. *Chem Soc Rev.* **2015**;44:8019–8061.
- [2] Chhatwal M, Mittal R, Gupta RD, et al. Sensing ensembles for nitroaromatics. *J Mater Chem C.* **2018**;6(45):12142–12158.
- [3] Shanmugaraju S, Mukherjee PS. Self-assembled discrete molecules for sensing nitroaromatics. *Chem–Eur J.* **2015**;21(18):6656–6666.
- [4] Kartha KK, Sandeep A, Praveen VK, et al. Detection of nitroaromatic explosives with fluorescent molecular assemblies and π -gels. *Chem Rec.* **2015**;15(1):252–265.
- [5] Shanmugaraju S, Mukherjee PS. π -Electron rich small molecule sensors for the recognition of nitroaromatics. *Chem Commun.* **2015**;51(89):16014–16032.
- [6] Grundlingh J, Dargan PI, El-Zanfaly M, et al. 2,4-Dinitrophenol (DNP): a weight loss agent with significant acute toxicity and risk of death. *J Med Toxicol.* **2011**;7(3):205–212.
- [7] Shanmugaraju S, Joshi SA, Mukherjee PS. Fluorescence and visual sensing of nitroaromatic explosives using electron rich discrete fluorophores. *J Mater Chem.* **2011**;21(25):9130–9138.
- [8] Moore DS. Instrumentation for trace detection of high explosives. *Rev Sci Instrum.* **2004**;75(8):2499–2512.
- [9] Shanmugaraju S, Dabadie C, Byrne K, et al. A supramolecular Troger's base derived coordination zinc polymer for fluorescent sensing of phenolic-nitroaromatic explosives in water. *Chem Sci.* **2017**;8(2):1535–1546.
- [10] Delente JM, Umadevi D, Shanmugaraju S, et al. Aggregation induced emission (AIE) active 4-amino-1,8-naphthalimide-Tröger's base for the selective sensing of chemical explosives in competitive aqueous media. *Chem Commun.* **2020**;56(17):2562–2565.
- [11] Chandrasekaran Y, Venkatramaiah N, Patil S. Tetraphenylethene-based conjugated fluoranthene: a potential fluorescent probe for detection of nitroaromatic compounds. *Chem–Eur J.* **2016**;22(15):5288–5294.
- [12] Kaur S, Gupta A, Bhalla V, et al. Pentacenequinone derivatives: aggregation-induced emission enhancement, mechanism and fluorescent aggregates for superamplified detection of nitroaromatic explosives. *J Mater Chem C.* **2014**;2(35):7356–7363.
- [13] Kartha KK, Sandeep A, Nair VC, et al. A carbazole–fluorene molecular hybrid for quantitative detection of TNT using a combined fluorescence and quartz crystal microbalance method. *Phys Chem Chem Phys.* **2014**;16(35):18896–18901.
- [14] Gupta SK, Kaleeswaran. D, Nandi S, et al. Bulky isopropyl group loaded tetraaryl pyrene based azo-linked covalent organic polymer for nitroaromatics sensing and CO₂ adsorption. *ACS Omega.* **2017**;2(7):3572–3582.
- [15] Lee YH, Liu H, Lee JY, et al. Dipyrrenylcalix[4]arene-a fluorescence-based chemosensor for trinitroaromatic explosives. *Chem Eur J.* **2010**;16(20):5895–5901.
- [16] Mosca L, Čejka J, Dolenský B, et al. Bowl-shaped Tröger's bases and their recognition properties. *Chem Commun.* **2016**;52(70):10664–10667.

- [17] Meher N, Iyer PK. Pendant chain engineering to fine-tune the nanomorphologies and solid state luminescence of naphthalimide AIEEgens: application to phenolic nitro-explosive detection in water. *Nanoscale*. **2017**;9(22):7674–7685.
- [18] Wang J, Yang Y, Sun G, et al. A convenient and universal platform for sensing environmental nitro-aromatic explosives based on amphiphilic carbon dots. *Environ Res*. **2019**;177:108621–108628.
- [19] Banerjee D, Hu Z, Li J. Luminescent metal–organic frameworks as explosive sensors. *Dalton Trans*. **2014**;43(28):10668–10685.
- [20] Guo L, Cao D. Color tunable porous organic polymer luminescent probes for selective sensing of metal ions and nitroaromatic explosives. *J Mater Chem C*. **2015**;3(33):8490–8494.
- [21] Yang J-S, Swager TM. Fluorescent porous polymer films as TNT chemosensors: electronic and structural effects. *J Am Chem Soc*. **1998**;120(46):11864–11873.
- [22] Zhang S, Yang Q, Wang C, et al. Porous organic frameworks: advanced materials in analytical chemistry. *Adv Sci*. **2018**;5:1801116–1801144.
- [23] Suresh VM, Bonakala S, Atreya HS, et al. Amide functionalized microporous organic polymer (Am-MOP) for selective CO₂ sorption and catalysis. *ACS Appl Mater Interfaces*. **2014**;6(7):4630–4637.
- [24] Shanmugaraju S, Umadevi D, Savyasachi AJ, et al. Reversible adsorption and storage of secondary explosives from water using a Tröger's base-functionalised polymer. *J Mater Chem A*. **2017**;5(47):25014–25024.
- [25] Guan X, Chen F, Fang Q, et al. Design and applications of three dimensional covalent organic frameworks. *Chem Soc Rev*. **2020**;49(5):1357–1384.
- [26] Xu Y, Jin S, Xu H, et al. Conjugated microporous polymers: design, synthesis and application. *Chem Soc Rev*. **2013**;42(20):8012–8031.
- [27] Banerjee S, Bright SA, Smith JA, et al. Supramolecular approach to enantioselective DNA recognition using enantiomerically resolved cationic 4-Amino-1,8-naphthalimide-based Tröger's bases. *J Org Chem*. **2014**;79(19):9272–9283.
- [28] Shanmugaraju S, McAdams D, Pancotti F, et al. One-pot facile synthesis of 4-amino-1,8-naphthalimide derived Tröger's bases *via* a nucleophilic displacement approach. *Org Biomol Chem*. **2017**;15(35):7321–7329.
- [29] Tanwar AS, Adil LR, Afroz MA, et al. Inner filter effect and resonance energy transfer based attogram level detection of nitroexplosive picric acid using dual emitting cationic conjugated polyfluorene. *ACS Sens*. **2018**;3(8):1451–1461.
- [30] Chen S, Yu Y-L, Wang J-H. Inner filter effect-based fluorescent sensing systems: A review. *Anal Chim Acta*. **2018**;999:13–26.
- [31] Zhao Y, Truhlar DG. The M06 suite of density functionals for main group thermochemistry, thermochemical kinetics, noncovalent interactions, excited states, and transition elements: two new functionals and systematic testing of four M06-class functionals and 12 other functionals. *Theory Chem Acc*. **2008**;120:215–241.
- [32] Frisch MJ, Trucks GW, Schlegel HB, et al., **2009**.
- [33] Roy B, Bar AK, Gole B, et al. Fluorescent Tris-imidazolium sensors for picric acid explosive. *J Org Chem*. **2013**;78(3):1306–1310.
- [34] Tanwar A, Meher N, Adil LR, et al. Stepwise elucidation of fluorescence based sensing mechanisms considering picric acid as a model analyte. *Analyst*. **2020**;145(14):4753–4767.